RSC Advances

PAPER

View Article Online
View Journal | View Issue

Cite this: *RSC Adv.*, 2017, **7**, 23591

Modeling and simulation of an improved ammonia-based desulfurization process for Claus tail gas treatment

Yuyin Tang,[ab] Yang Gao,[c] Dan Liu,[b] Fenglian Zhang,[b] Siqiu Qu,[c] Zhengping Hao,[bd] Xin Zhang*[bd] and Zhao-Tie Liu *[a]

Received 25th February 2017
Accepted 25th April 2017

DOI: 10.1039/c7ra02343j

rsc.li/rsc-advances

An improved ammonia-based desulfurization technology was proposed, in which the produced excess NH_4HSO_3 was concentrated by using the heat from the Claus tail gas and then SO_2 was recovered by decomposing the concentrated NH_4HSO_3 in the Claus furnace. Furthermore, the process was modeled and simulated using the commercial software Aspen Plus. The characteristics of the ammonia-based desulfurization model were validated and compared with experimental results. Moreover, the water balance in the system was maintained, therefore, no extra water was required. Under the water balance condition, the SO_2 removal performance in the system was predicted with various operating conditions. The model exhibited a reliable prediction of the desulfurization performance of the innovative process, which will be favorable for actual industrial application.

1 Introduction

Nowadays, coal chemical industries are playing a more and more important role due to economic development and the increasingly serious energy crisis. However, during the coal chemical production process, a large amount of H_2S, which is one of the most toxic environmental pollutants, is produced.[1,2] Therefore, it must be appropriately treated and removed prior to emission. Currently, the Claus process is one of the most important and widely used technologies to recover elemental sulfur from H_2S-containing gases.[3,4] Nevertheless, the sulfur recovery efficiency is only 90–96% for two-stage Claus reactors and 95–98% for three stage Claus reactors,[5–8] due to the thermodynamic limitations of the Claus equilibrium reaction. Thus, there are still 2–3% of sulfur compounds (elemental sulfur vapor, COS, CS_2, SO_2 and H_2S) left in Claus tail gas. From the viewpoint of environmental protection, the Claus tail gas must be seriously considered and treated before discharge into the atmosphere.

As is known, the remaining H_2S in Claus tail gas can be eliminated to a great extent by various additional purification technologies (such as low temperature Claus technology,[9,10] reduction–absorption technology[11] and H_2S selective oxidation technology[12–15]). Even though additional purification technologies are applied, the sulfur recovery can only reached as high as 99%. On the other hand, SO_2 emission restriction has become increasingly stringent. The Chinese government had enforced the new emission standards of pollutants for petroleum chemical industry in 2015, wherein SO_2 emission has been restricted for 100 mg m^{-3} and 50 mg m^{-3} for special regions. It is significantly indicated that the emission cannot meet the new standard even the Claus tail gas is treated by the mentioned additional process. On this occasion, various absorption technologies, such as CaO,[16–18] MgO[19–21] and NH_3 (ref. 22–24) based desulfurization processes, are seriously considered as the potential candidate for Claus tail gas treatment due to the higher sulfur removal efficiency (can reach almost 100%) and low cost. In these absorption technologies, all sulfur compounds are firstly transformed into SO_2 after Claus reaction. Subsequently, SO_2 is further absorbed by alkaline absorbents and transformed into useful byproducts. Among them, NH_3 based desulfurization process is the most promising one, taking into account that NH_3 can be easily obtained in coal chemical industries. However, in the case of traditional ammonia-based desulfurization process, a tail gas cooling system is required to cool the fuel gas, which wastes a lot of water and energy. Furthermore, the produced excess $(NH_4)_2SO_3$ and NH_4HSO_3 are oxidized and crystallized to $(NH_4)_2SO_4$ chemical fertilizer by a long and complex process along with a large consumption of heat. Meanwhile, a large amount of extra water is consumed during the SO_2 absorption reaction.

[a]*Key Laboratory of Applied Surface and Colloid Chemistry, School of Chemistry and Chemical Engineering, Shaanxi Normal University, Xi'an, 710119, China. E-mail: ztliu@snnu.edu.cn; Fax: +86-29-81530802; Tel: +86-29-81530802*

[b]*Department of Environmental Nano-materials, Research Center for Eco-Environmental Sciences, Chinese Academy of Sciences, Beijing 100085, China. E-mail: zhangxin@rcees.ac.cn; Tel: +86-10-62843688*

[c]*Center of Research & Development, Shandong Sunway Petrochemical Engineering Share Co., Ltd, Beijing 100015, China*

[d]*National Engineering Laboratory for VOCs Pollution Control Material & Technology, Beijing 101408, China*

Therefore, from the viewpoint of practice, the production of $(NH_4)_2SO_4$ byproducts makes the tail gas treatment process rather complex and further increases the operating costs. Moreover, the storage, transportation and sale of byproducts formed in absorption process are still serious problems.

On basis of this, an improved ammonia-based desulfurization technology is tentatively proposed taking into account of the tail gas composition in coal chemical industry, usually 25% H_2O, 24% CO_2, 50.5% N_2 and 0.5% SO_2. In the process, the produced excess NH_4HSO_3 is concentrated using the heat from the Claus tail gas, which also plays the role of cooling system. And then, the NH_4HSO_3 solution is recycled to the Claus furnace. Wherein, NH_4HSO_3 is decomposed into SO_2, N_2 and H_2O. Subsequently, SO_2 participates in the Claus reaction. Therefore, the process is shorter, heat saving and has no byproduct. It is worth mentioning that extra water for absorption reaction is not required due to the large amount of water in tail gas. More importantly, the purified gas must be maintained at a special temperature in order to take away the excess water in tail gas after absorption reaction, *i.e.*, maintained the water balance of the system. Otherwise, the sulfur removal efficiency will decrease drastically. Additionally, a water spray column is designed to remove the escaped NH_3 as well as the trace SO_2 in purified gas.

In the present paper, the SO_2 absorption and NH_4HSO_3 concentrating under the water balance condition was modeled and simulated by the commercial software Aspen Plus. Moreover, the characteristics of ammonia-based desulfurization process was also studied and compared with experimental results. Additionally, the impact of various operating parameters on SO_2 removal efficiency was examined. All in all, the desulfurization performance of the innovated process can be predicted reliably, which is favorable for the actual industrial application.

2 Computational details

2.1 Process description

A second-stage ammonia-based desulfurization system with a prewashing step was developed. The prewashing step was designed to cool the tail gas as well as to concentrate the produced excess NH_4HSO_3. The process is shown in Fig. 1, including a SO_2 absorbing column, a washing column, a prewashing column, a mixer and a stream splitter. To simplify the process, the fluid transportation units are omitted, and the pressure of the system is considered stable at 100 kPa and without any pressure drop.

In the present process, the tail gas (TAILGAS) containing a mixture of 25% H_2O, 24% CO_2, 50.5% N_2 and 0.5% SO_2 was firstly introduced to the prewashing column from the bottom, while the rich NH_4HSO_3 solution (RICH) entered from the top of the column. In this heat transfer process, the tail gas was cooled and partial water in the rich liquid was evaporated into the gas phase, *i.e.*, the rich liquid NH_4HSO_3 was concentrated. And then, the concentrated NH_4HSO_3 absorption liquid (PRODUCT) was transferred to Claus furnace, while the cooled tail gas (GASIN) sequentially entered the absorbing column

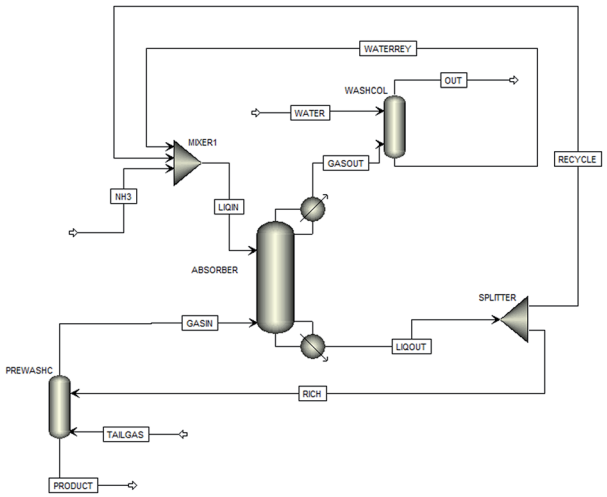

Fig. 1 Process for desulfurization system with a prewashing system.

(ABSORBER) from the bottom. SO_2 was absorbed by the $(NH_4)_2SO_3$-rich solution (LIQIN), which was sprayed from the top of the absorbing column. The NH_4HSO_3-rich solution (LIQOUT) was collected at the bottom of the column. Partial rich solution was regenerated by the mixture of the production of the washing column and ammonia gas, and recycled back to the absorbing column. Meanwhile, the excess rich solution was transferred to the prewashing column and participated in the mentioned heat transfer process. However, the process must be operated at a relatively high temperature due to the requirement of water balance, which facilitated the ammonia escape. Thus, a washing column was designed to inhibit the ammonia escape. Escaped ammonia was absorbed by the sprayed water in the washing column, and the produced ammoniated water was reused in the above mentioned regeneration step associate with ammonia. A mixer (MIXER) was included in the desulfurization model to control the flow rate and composition of the lean solution in the SO_2 absorber.

2.2 Absorption reaction model of SO_2

The reactions that are mainly occurred during the SO_2 absorption reaction are shown in Table 1. The chemical absorption

Table 1 Reaction model for the NH_3–SO_2–CO_2–H_2O system

Reaction no.	Type	Chemical equation
1	Equilibrium	$H_2O \leftrightarrow OH^- + H^+$
2	Equilibrium	$H_2O + NH_3 \leftrightarrow NH_4^+ + OH^-$
3	Equilibrium	$H_2O + SO_2 \leftrightarrow H^+ + HSO_3^-$
4	Equilibrium	$HSO_3^- \leftrightarrow H^+ + SO_3^{2-}$
5	Equilibrium	$H_2O + CO_2 \leftrightarrow H^+ + HCO_3^-$
6	Equilibrium	$HCO_3^- \leftrightarrow H^+ + CO_3^{2-}$
7	Salt	$NH_4HSO_3 \leftrightarrow NH_4^+ + HSO_3^-$
8	Salt	$(NH_4)_2SO_3 + H_2O \leftrightarrow H_2O + 2NH_4^+ + SO_3^{2-}$
9	Salt	$(NH_4)_2SO_3 \leftrightarrow 2NH_4^+ + SO_3^{2-}$
10	Salt	$NH_4HCO_3 \leftrightarrow NH_4^+ + HCO_3^-$

process of SO_2 by ammonia-based solution was similar to physical absorption process, and conformed to two-film theory. SO_2 was firstly transferred from the gas phase into the liquid-film, and then into the liquid phase. And then, SO_2 reacted with the absorbent instantaneously when it entered the liquid phase, which enlarged the solubility of SO_2 in liquid phase as well as enhanced the absorption driving force. Consequently, SO_2 concentration dropped sharply in the liquid phase due to the reactions, which decreased the mass transfer resistance, increased the coefficient of absorption and ultimately improved the absorption efficiency.

According to the theory of chemical absorption, SO_2 reacted with the absorbent instantaneously when it entered the liquid phase, therefore the partial pressure of SO_2 on the gas–liquid interface was infinitely close to 0. The diffusion resistance of gas film was the rate-determining step of absorption reaction.

2.3 Rate kinetics of the simulation

During the simulation, SO_2 and CO_2 reacted with the ammonia solution and formed NH_4HSO_3, $(NH_4)_2SO_3$, NH_4HCO_3, $(NH_4)_2CO_3$ and $(NH_4)_2SO_3 \cdot H_2O$. The gas reaction between NH_3, SO_2 and CO_2 was ignored during the simulation. The equilibrium constants (K) used for the reactions were calculated by using the following rate equation:

$$\ln K = A + \frac{B}{T} + C \ln T + DT \quad (1)$$

where T stands for absolute temperature (K). The model specifications and parameters A, B, C and D are available in the Aspen databank, and are listed in Table 2.

The rate-based RadFrac model was adopted for the absorbing, prewashing and washing column. The rate-based approach uses the Maxwell–Stefan model to compute the multicomponent mass transfer, including the use of binary coefficients to evaluate the mass transfer rates between the vapor and liquid phases.[25] The absorption is based on the two-film theory,[26] wherein the mass transfer resistance was concentrated in a thin layer adjacent to the bulk phase boundary. The discretized film equations are combined with the heat and mass balance at each stage to obtain an accurate temperature and concentration profile over the entire column.[27]

The mixed flow model was selected for the three columns, in which the bulk properties of each phase are assumed to be the same as the outlet conditions for that phase. Wegstein method was employed to solve the system of algebraic equations. The electrolyte NRTL model was selected as the thermo physical properties of the system, by which the thermodynamic properties of the liquid phase were determined. Henry's law was applied on N_2, NH_3, CO_2 and SO_2. The Henry's law constants of SO_2, NH_3 and CO_2 in water were taken from Meyer *et al.*,[28] Que *et al.*[29] and Yan *et al.*[30]

The coefficients used for temperature-dependent physical properties of model components were taken from the Design Institute for Physical Properties and the Aspen Plus data system. The molar volume of the electrolyte solution was calculated basing on the Clarke aqueous electrolyte volume model. The liquid viscosity was determined by the Jones–Dole model. The Riedel model was adopted to calculate the thermal conductivity coefficients of the electrolyte solution. The diffusion coefficients were computed basing on the Nernst–Hartley model, and the surface tension of the aqueous electrolyte solution was calculated using the Onsager–Samaras model.

Table 2 Reaction parameters for the NH_3–SO_2–CO_2–H_2O system

Parameter	A	B	C	D
Reaction 1	132.9	-1.345×10^4	−22.48	0
Reaction 2	−1.257	−3335	1.497	−0.03706
Reaction 3	−5.979	637.4	0	−0.01513
Reaction 4	−25.29	1333	0	0
Reaction 5	231.5	-1.209×10^4	−36.78	0
Reaction 6	216.1	-1.243×10^4	−35.48	0
Reaction 7	−1.962	637.4	0	−0.01513
Reaction 8	−1297	3.347×10^4	224.2	−0.3516
Reaction 9	920.4	-4.450×10^4	−139.3	0.03619
Reaction 10	554.8	-2.244×10^4	−89.01	0.06473

3 Results and discussion

3.1 Model validation

The validation experiments were carried out on special manufactured equipment. The experimental procedure was consistent with the established model. Additionally, pumps and fans were added in the experiments to transport liquid and gas phases. In the experiments, the composition and concentration of the absorbent was adjusted by adding ammonia gas, SO_2 and $(NH_4)_2SO_3$ to the solution. The experiments were conducted under the same conditions (pH, absorbent temperature, initial total salt concentration, gas volumetric flow, SO_2 concentration) with the simulation. SO_2 concentration, the pH, composition, and concentration of the absorbent solution were determined after the system was in equilibrium for at least 5 min. In the experiment, the concentration of the absorbent (NH_4HSO_3, $(NH_4)_2SO_3$) was determined by an iodometry method and acid–base neutralization titration. Each sample was titrated in triplicate. The SO_2 concentration was measured by an Infrared Flue

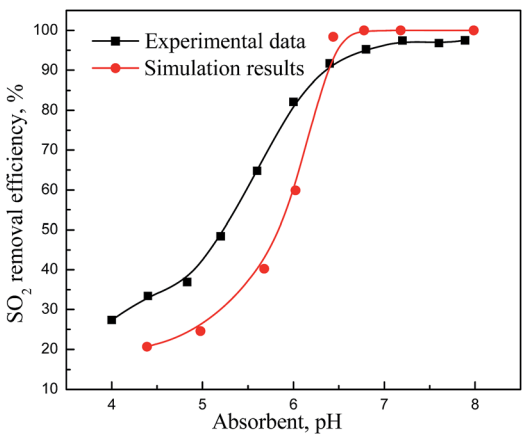

Fig. 2 Simulation and experimental results of SO_2 removal efficiency with different absorbent pH.

Gas Analyzer. The experiments were carried out under the condition of 5000 ppm SO_2, initial total salt concentration 0.6 mol L^{-1}, gas volumetric flow 8 m^3 h^{-1}, liquid–gas ratio 8 L m^{-3}, absorbent pH 6.7 and absorbent temperature 40 °C.

The simulated SO_2 removal results were verified at different operating conditions (pH, liquid–gas ratio (L/G), SO_2 concentration, absorbent temperature and absorbent concentration) against experimental results. The operating parameters of the Aspen Plus model were set as the same as the experimental conditions. Moreover, the water balance of the system was not considered in this situation.

Fig. 2 shows the relationship between SO_2 removal efficiency and the absorbent pH. The absorbent pH during the experiment was adjusted by adding SO_2 or NH_3 into the solution, while the absorbent pH during the simulation was adjusted by changing the concentration of $(NH_4)_2SO_3$ and NH_4HSO_3 of the inlet streams. It can be seen that the simulation results agreed well with the experimental data. Both results revealed that the SO_2 removal efficiency increased with the rise of absorbent pH. The SO_2 removal efficiency of experimental data and simulation result around pH = 4 was 27.3% and 20.6%, respectively. And then, the SO_2 removal efficiency rose sharply when the pH reached to 6. The SO_2 removal efficiency could attain as high as 98% at pH = 6.4. Furthermore, the SO_2 removal efficiency kept almost steady when pH was higher than 6.5. The pH of absorbent reflects the composition of the absorbent. A lower pH indicates a lower concentration of $(NH_4)_2SO_3$ and a higher concentration of NH_4HSO_3, which not only obstructs the SO_2 absorption reaction, but ionizes H^+ ion, inhibiting the dissolution of SO_2 into the water. The combined affection leads to a lower SO_2 removal efficiency at low pH levels. When pH is higher than 6.5, the absorbent is meanly composed of $(NH_4)_2SO_3$, and the SO_2 absorption rate is mainly controlled by the mass transfer rate instead of solution composition. It means that the continually increase of pH had little impact on the SO_2 removal efficiency, but greatly increased the operating cost. The pH of the absorbent should be kept between 6 and 7. As a buffer solution, the composition and the concentration of $(NH_4)_2SO_3$–NH_4HSO_3 system varies even with the same solution pH. Due to the difficulty of controlling both the absorbent concentration and solution pH at the same time, the experimental results showed some variations in absorbing capacities.

Liquid–gas ratio (L/G) is an influencing factor that can decide the size of the absorption equipment and influence the operating cost. With a larger L/G ratio, the driving force of absorption enhances, which is in favor of absorption progress, but at the same time increases the operating cost. Fig. 3 illustrated the effect of liquid–gas ratio (L/G) on SO_2 removal efficiency. Both curves exhibited consistent regime. It is significantly noted that the SO_2 removal efficiency increased with the increase of liquid–gas ratio. The SO_2 removal efficiency was only 26% when the liquid–gas ratio was 2. However, the SO_2 removal efficiency increased sharply to 83.6% with the rise of liquid–gas ratio to 4. The growth rate decreased when the liquid–gas ratio exceeded 4. It can be explained by the fact that the absorbent was initiatorily insufficient. Therefore, the increase of liquid–gas ratio implied the increase of the liquid flow rate entering the absorbing system, which increased the contact of gas–liquid. Simultaneously, the mass transfer force increased, which was beneficial to more SO_2 in gas phase entering liquid phase.

The influence of different SO_2 inlet concentration on SO_2 removal efficiency is depicted in Fig. 4. It is noteworthy that the simulation results and experimental results exhibit remarkably different variation trend with respect to the rise of SO_2 concentration. In the simulation results, the SO_2 removal efficiency kept almost stable at 98% when the SO_2 concentration rose from 2000 to 15 000 ppm. Whereas, the SO_2 removal efficiency dropped sharply to 86% with a further rise of SO_2 concentration. Conversely, in experimental results, the SO_2 removal efficiency gradually dropped from 100% to 86% with a rise of SO_2 concentration. This difference can be attributed to the fact that the simulated process was conducted in a rather ideal condition, *i.e.*, the two phases in tower are uniform distributing and well intermixed, which assures a better reaction completion. Moreover, the SO_2-absorption process is a gas-film controlled process, in which the gas film resistance decides the reaction rate and degree. Therefore, the initiate increase of

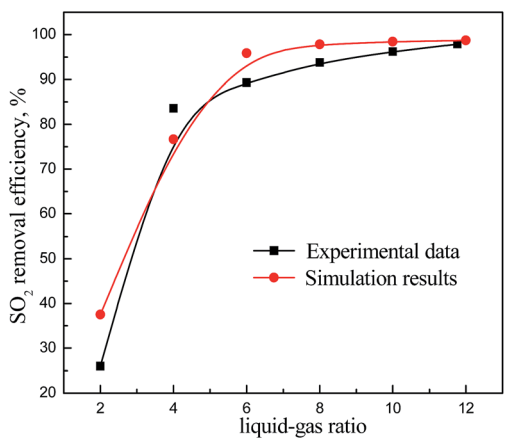

Fig. 3 Simulation and experimental results of SO_2 removal efficiency with different liquid–gas ratio.

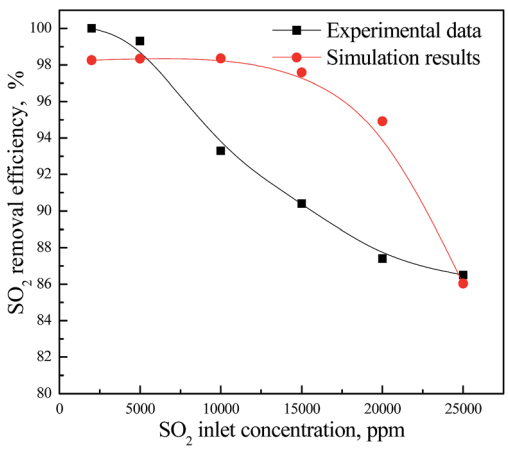

Fig. 4 Simulation and experimental results of SO_2 removal efficiency with different SO_2 inlet concentration.

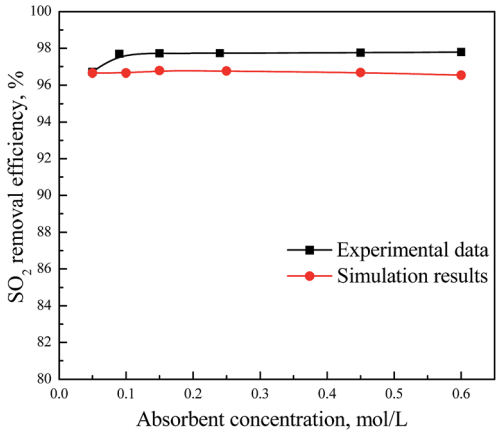

Fig. 5 Simulation and experimental results of SO_2 removal efficiency with different absorbent concentration.

SO_2 inlet concentration improves the mass transfer driving force, leading to the rise of SO_2 absorbing capacity. Hence, the SO_2 removal efficiency can be maintained in the simulated process. The gradual decrease of SO_2 removal efficiency in experimental data can be attributed to the insufficiency of the gas–liquid contact, actually. SO_2 molecules cannot reach the gas–liquid interface before they were carried out by the gas stream, causing the gradual decrease of SO_2 removal efficiency.

Fig. 5 shows the effect of the absorbent $(NH_4)_2SO_3$ concentration on the SO_2 removal efficiency. It can be noted that the simulation results agreed well with the experimental data. Both results revealed that the SO_2 removal efficiency was almost maintained at 97% with the rise of $(NH_4)_2SO_3$ concentration. It can be explained that the absorbent was $(NH_4)_2SO_3$-excess in the process. Therefore, the absorption rate was mainly determined by the mass transfer rate between gas and liquid. Thus the increasing $(NH_4)_2SO_3$ concentration can hardly improve the SO_2 removal efficiency.

In the experiments, the existence of the fluid transportation units can act as fans and pumps. Namely, the experiments are operated under a micro positive pressure, *i.e.*, the experimental pressure is always a little higher than the simulated process. As known a higher operating pressure is beneficial to the absorbing process. Therefore, under the same operating conditions, the desulfurization efficiencies of experiments are higher than simulated results.

Particularly, almost all the single factor simulation results are extremely consistent with the experimental results. Therefore, it can be considered that the developed model can predict the desulfurization performance of the innovated process reliably.

3.2 Desulfurization performance simulation

The desulfurization performance of the innovated process was simulated by the developed and validated model. The simulation condition and results were collected in Tables 3 and 4, respectively. Especially, all the simulations were conducted based on the water balance of the system (the purified gas was controlled at 70.4 °C). Moreover, the SO_2 removal efficiency can attain as high as 96%.

3.2.1 Water balance of the system. As mentioned above, the process must be operated under the condition of water balance. Otherwise, the SO_2 removal efficiency will decrease drastically and further increase the operation cost. For the

Table 3 Model parameters and operating conditions

Units	Specifications	Operating conditions
Prewashing column	Calculation type: RadFrac model Flow model: mixed Height: 500 mm Diameter: 100 mm Packing type: Raschig rings 13 mm	Operating pressure: 100 kPa Enrichment stream flow rate: 0.71 L h^{-1} Enrichment stream temperature: 70 °C Tail gas flow rate: 8 m^3 h^{-1} Tail gas temperature: 160 °C CO_2 concentration in tail gas (v/v%): 24 Water vapor concentration (v/v%): 25.5 SO_2 volume fraction (ppm): 5000
SO_2 absorber	Calculation type: RadFrac model Flow model: mixed Height: 1000 mm Diameter: 100 mm Packing type: Raschig rings 13 mm	Operating pressure: 100 kPa Lean solution flow rate: 7.13 L h^{-1} Lean solution temperature: 70.2 °C
Washing column	Calculation type: RadFrac model Flow model: mixed Height: 500 mm Diameter: 100 mm Packing type: Raschig rings 13 mm	Operating pressure: 100 kPa Inlet temperature of wash water: 25 °C Wash water flow rate: 0.75 L h^{-1}
Mixer	Type: Stream mixer Valid phase: vapor–liquid	Operating pressure: 100 kPa NH_3 flow rate: 1.28 mol h^{-1} NH_3 temperature: 25 °C
Splitter	Valid phase: vapor–liquid Recycle flow split ratio: 0.9	Operating pressure: 100 kPa

Table 4 Simulation results with water balance

Stream name							
Simulation results	TAILGAS	NH_3	WATER	OUT	PRODUCT	RECYCLE	ENRICH
Temperature/°C	160.0	25.00	25.00	70.55	70.29	70.21	70.21
Pressure/kPa	101.0	101.0	101.0	100.0	100.0	100.0	100
Vapor/frac	1.000	1.000	0	1.000	0	0	0
Mole flow/mol h^{-1}	224.6	1.280	41.51	239.6	26.76	319.9	35.54
Mass flow/kg h^{-1}	6.633	0.02180	0.7479	6.854	0.5494	6.285	0.6985
Volume flow/L h^{-1}	8000	31.19	0.7500	6828	0.5734	6.377	0.7085
Enthalpy/Gcal h^{-1}	-8.160×10^{-3}	-1.400×10^{-5}	-2.800×10^{-3}	-9.200×10^{-3}	-1.85×10^{-3}	−0.02188	-2.400×10^{-3}
pH			7.00		5.12	5.90	5.90
Mole/frac							
NH_3	0	1	0	5.740×10^{-4}	2.620×10^{-5}	9.340×10^{-5}	9.340×10^{-5}
SO_2	5.000×10^{-3}	0	0	2.300×10^{-4}	1.770×10^{-5}	1.520×10^{-6}	1.520×10^{-6}
CO_2	0.2400	0	0	0.2250	5.030×10^{-5}	4.890×10^{-5}	4.890×10^{-5}
N_2	0.5050	0	0	0.4734	2.950×10^{-6}	2.990×10^{-6}	2.990×10^{-6}
WATER	0.2500	0	1	0.3008	0.9173	0.9411	0.9411
NH_4^+	0	0	0	0	4.266×10^{-2}	3.277×10^{-2}	3.277×10^{-2}
H^+	0	0	1.810×10^{-9}	0	2.300×10^{-7}	4.070×10^{-8}	4.070×10^{-8}
HCO_3^-	0	0	0	0	1.260×10^{-5}	7.320×10^{-5}	7.320×10^{-5}
OH^-	0	0	1.810×10^{-9}	0	9.640×10^{-10}	5.530×10^{-9}	5.530×10^{-9}
HSO_3^-	0	0	0	0	3.713×10^{-2}	1.921×10^{-2}	1.921×10^{-2}
CO_3^{2-}	0	0	0	0	1.240×10^{-9}	3.770×10^{-8}	3.770×10^{-8}
SO_3^{2-}	0	0	0	0	2.759×10^{-3}	6.743×10^{-3}	6.743×10^{-3}

Table 5 The mole flow of water entering and leaving the system

	Inlet streams		Outlet streams	
Stream	TAILGAS	WATER	OUT	PRODUCT
H_2O mole flow/mol h^{-1}	56.15	41.51	72.06	24.53

present simulation, water in the system can be classified into three kinds: water of entering the system, water of leaving the system and reacted water. Water of entering the system is mainly originated from the water scrubbing step (using to catch the escaped ammonia) and the TAILGAS (containing about 24% H_2O), while it leaves the system by the outlet streams PRODUCT and OUT. The amount of water participated in the reactions can be calculated by the changes of the concentration of HSO_3^-, SO_3^{2-}, HCO_3^-, and CO_3^{2-} in the liquid phase entering (WATER) and leaving (PRODUCT) the system according to reactions (1) to (10). The mole flow of water in the inlet and outlet streams are shown in Table 5, and the water consumption of the reactions is shown in Table 6.

Table 6 Water consumption of reactions in the system

Mole flow/mol h^{-1}	WATER stream	PRODUCT stream	Increase of the ion
SO_3^{2-}	0	0.07393	0.07393
HSO_3^-	0	0.9937	0.9937
CO_3^{2-}	0	3.330×10^{-8}	3.300×10^{-8}
HCO_3^-	0	3.400×10^{-4}	3.400×10^{-4}

The consumption of water can be calculated as:

$$n(H_2O) = \Delta n(SO_3^{2-}) + \Delta n(HSO_3^-) + \Delta n(CO_3^{2-}) + \Delta n(HCO_3^-) = 1.068 \text{ mol } h^{-1}$$

The amount of water entering the system should keep balance with the amount of water leaving the system and participating in the reactions. The water balance equation can be presented as:

$$n(H_2O\text{-WATER}) + n(H_2O\text{-TAILGAS}) = n(H_2O\text{-PRODUCT}) + n(H_2O\text{-GASOUT}) + \Delta n(H_2O\text{-consumption})$$

$$\Delta n(H_2O) = \Delta n(H_2O\text{-WATER}) + \Delta n(H_2O\text{-TAILGAS}) - \Delta n(H_2O\text{-PRODUCT}) - \Delta n(H_2O\text{-GASOUT}) - \Delta n(H_2O\text{-consumption}) = 0.0109 \text{ mol}$$

It positively means that the increased amount of water in the system was only 0.0109 mol h^{-1}, which can be neglected. Therefore, it is considered that the water balance of the system is reached.

3.2.2 Effect of tail gas temperature on SO_2 removal efficiency. Due to the easy volatility of NH_3 and easy decomposition of $(NH_4)_2SO_3$ and NH_4HSO_3, most of the ammonia-based desulfurization processes are carried out at low temperatures and the temperature of the inlet gas is usually controlled at 60–80 °C. In the present process, the tail gas is cooled by the rich

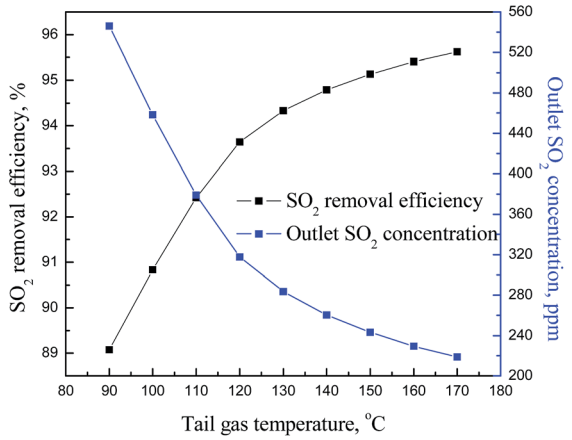

Fig. 6 Simulation results of SO_2 removal efficiency with different tail gas temperature.

liquid. The impact of tail gas temperature on SO_2 removal efficiency in the ranges of 90 to 170 °C is shown in Fig. 6. It can be clearly observed that the SO_2 removal efficiency increased from 89 to 95.6% along with the tail gas temperature increased from 90 °C to 170 °C.

During the course of absorption process, the rise of inlet tail gas temperature can hardly influence the liquid phase temperature due to the notably difference of specific heat capacity. Thus, the differences in temperature between gas and liquid phase were increased. Subsequently, the mass transfer driving force was increased. On the other hand, the composition of the absorption solution varied with different inlet tail gas temperatures. A higher inlet tail gas temperature can induce the increase of reaction rate, therefore the SO_2 absorption capacity increased. Notably, the SO_2 absorption capacity was the rate-determining step in the absorption reaction according to the two-film theory. Therefore, the increase of tail gas temperature induced the increase of SO_2 remove efficiency.

3.2.3 Effect of introduced water temperature on SO_2 removal efficiency. As is known, the introduced water was used to catch the escaped ammonia and further used to regenerate the absorption solution. Therefore, the absorbent temperature varies with the rise of introduced water temperature. On the other hand, the absorbent temperature is an influential parameter that affects the diffusion rates, mass transfer and reaction kinetics. Fig. 7 shows the effect of introduced water temperature on SO_2 removal efficiency. It can be seen that the SO_2 removal efficiency was decreased slightly from 95.5 to 95% when the temperature of introduced water was rose up to 50 °C. Thus, it indicates that the introduced water temperature can hardly influence the SO_2 removal efficiency, which be explained by the fact that the flow rate of the introduced water was rather small compared with the flow rate of lean solution stream, *i.e.* the temperature of introduced water has little impact on the absorbent temperature.

3.2.4 Effect of the volume flow rate of NH_3 on SO_2 removal efficiency. Fig. 8 shows the effect of the volume flow rate of NH_3 added to the system on SO_2 removal efficiency. During the course of experiment, the SO_2 removal efficiency was only 43.61% when the volume flow of NH_3 was 12.2 L h^{-1}. And the concentration of SO_2 and NH_3 in the outlet gas was 2656 and 15 ppm, respectively. However, the SO_2 removal efficiency was raised sharply to 93.75% with the volume flow of NH_3 increased to 29.2 L h^{-1}. Meanwhile, the concentration of SO_2 in the outlet gas exhibited a remarkably decline to 293 ppm, and the concentration of NH_3 rose slightly to 334 ppm. After that, the increase of ammonia volume flow had little positive impact on the SO_2 removal efficiency and the concentration of SO_2 in the outlet gas, which moved from 93.75 to 97.3%. Thus the volume flow rate of ammonia should be kept at the ranges of 30 to 35 L h^{-1}. The continue increase of ammonia flow rate cannot improve the SO_2 removal efficiency but would result in an increase in the ammonia waste and operating cost.

3.2.5 Effect of CO_2 fraction on SO_2 removal efficiency. The tail gas contains large quantities of CO_2, which can also be absorbed by the ammonia-based solution, and worsen the SO_2 removal efficiency. Therefore, the effect of CO_2 fraction on SO_2 removal efficiency was studied. The results are shown in Fig. 9. It is significant to observe that the SO_2 removal efficiency was decreased slightly from 95.45% to 95.35% when the CO_2 fraction increased from 8 to 36%. Meanwhile, the CO_2 removal

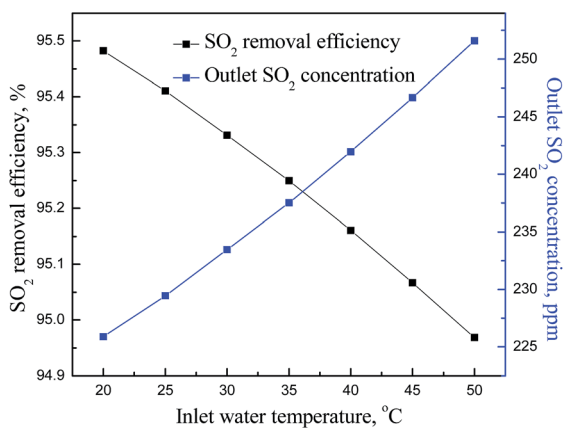

Fig. 7 Simulation results of SO_2 removal efficiency with different water temperature.

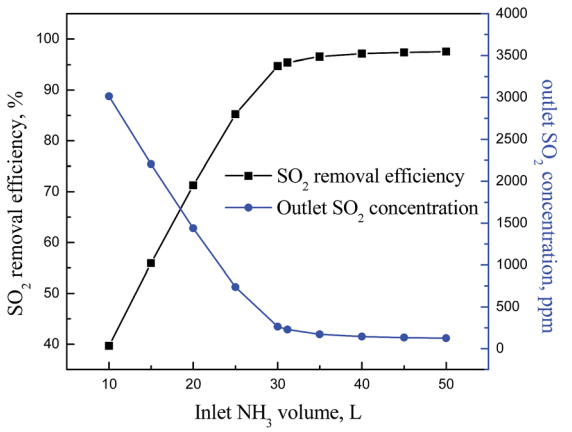

Fig. 8 Simulation results of SO_2 removal efficiency with different inlet NH_3 volume.

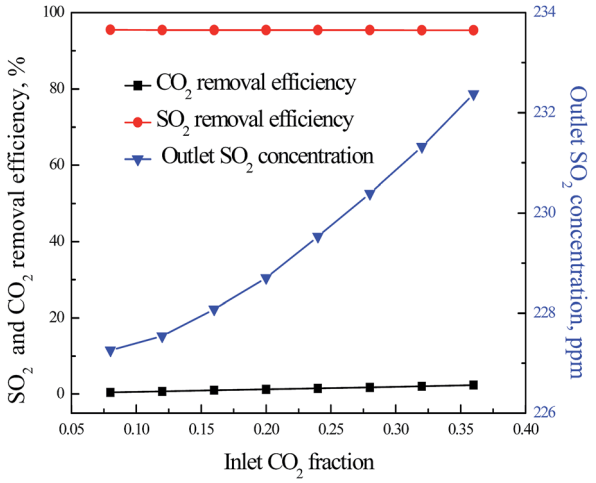

Fig. 9 Simulation results of CO_2 fraction on SO_2 removal efficiency.

efficiency was maintained at a rather low level. Therefore, it is illustrated that the CO_2 fraction has little effect on SO_2 removal.

3.2.6 Ammonia escape. The escape of ammonia in the system is depended on several operating parameters, *i.e.* inlet tail gas temperature, introduced water temperature, introduced water flow rate and inlet NH_3 flow rate. The influence of these parameters on ammonia escape is shown in Fig. 10. It can be noted that the ammonia escape from the column decreased slightly from 576 to 559 ppm when the introduced water temperature rose from 20 to 50 °C. And the ammonia escape increased from 115 to 661 ppm when the gas temperature was raised from 90 to 170 °C. Meanwhile, by increasing the introduced water flow rate from 0.5 to 4 L h^{-1}, the ammonia escape in the outlet gas increased linearly from 514 to 671 ppm. However, the ammonia outlet concentration increased exponentially from 15 to 7347 ppm when the inlet NH_3 flow rate increased from 12 to 73 mol L^{-1}. Therefore, the ammonia escape decreased with the rise of introduced water temperature. Moreover, it increased with the rise of tail gas temperature, introduced water flow rate and inlet NH_3 flow rate.

4 Conclusions

An improved ammonia-based desulfurization technology was tentatively proposed, wherein the produced excess NH_4HSO_3 was concentrated using the heat from the Claus tail gas and SO_2 was recovered by decomposing the concentrated NH_4HSO_3 in the Claus furnace. Furthermore, the process was modeled and simulated using the commercial software Aspen Plus. The characteristics of ammonia-based desulfurization model was validated and compared with experimental results. Moreover,

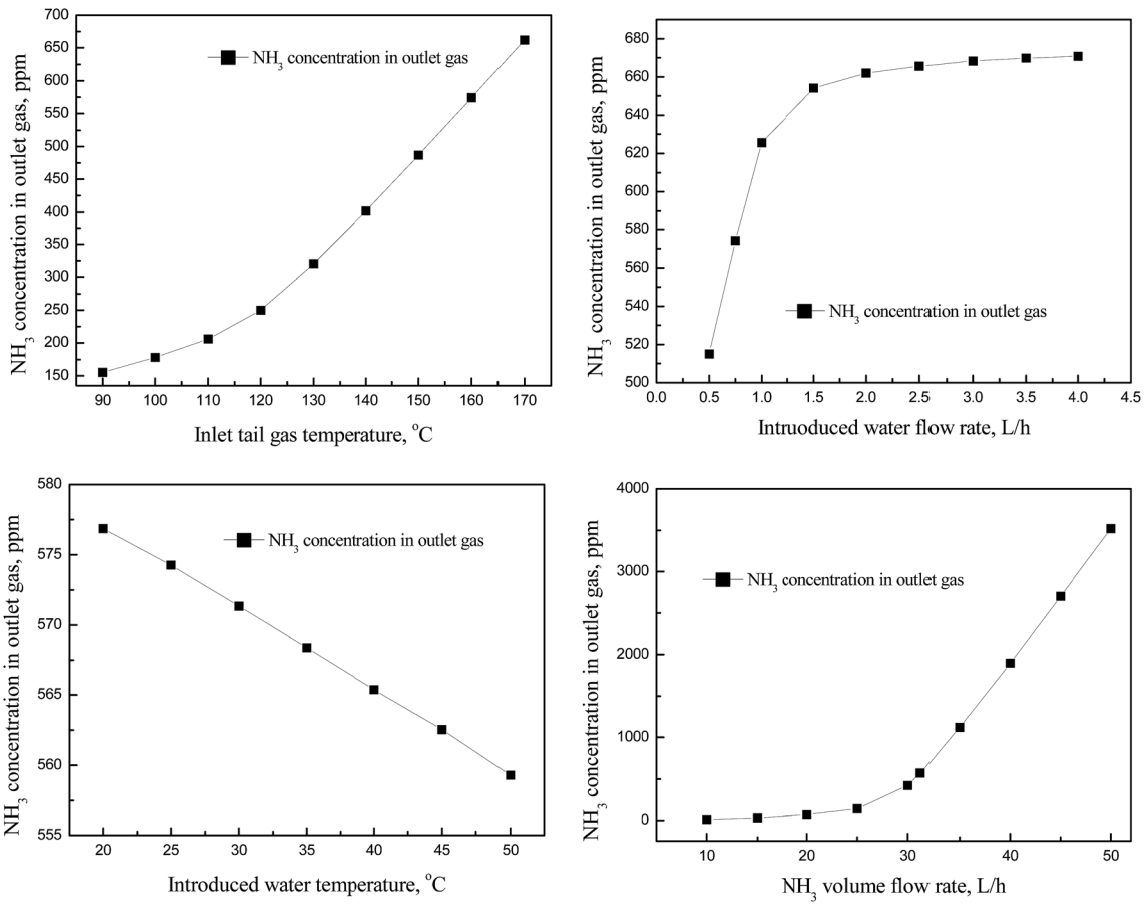

Fig. 10 Effect of operating conditions on ammonia escape.

the water balance in the system must be maintained, therefore, no extra water was required. Under the water balance condition, the SO_2 removal performance of the system was predicted with various operating conditions. It revealed that the SO_2 removal efficiency increased slightly with the rise of tail gas temperature and introduced water temperature. Oppositely, it increased remarkably with the rise of NH_3 flow rate. Particularly, the effect of CO_2 fraction on SO_2 removal efficiency can be ignored. And the ammonia escape of the system was appropriately inhibited. The model exhibited a reliable prediction on the desulfurization performance of the improved process, which was favorable for the actual industrial application.

The main starting point of the modified process was the realization of elemental sulfur recovery. Therefore, the excess concentrated NH_4HSO_3 was transferred to the Claus furnace and further decomposed to SO_2 and H_2O. However, the Claus reaction was thermodynamic equilibrium limited ($2H_2S + SO_2 \rightarrow 3S + H_2O$). Thus, the large extra amount H_2O entering the furnace can play a negative effect to the reaction, causing the decrease of Claus reaction efficiency. Hence, realizing the rational integration of the modified process and Claus process was the most crucial challenge for the further application of this process.

Acknowledgements

This work was financially supported by the National Natural Science Foundation (21577158, 21507148, 21327011) and the Strategic Priority Research Program of the Chinese Academy of Sciences (XDB05050200).

References

1 J. Abbasian and R. B. Slimane, *Ind. Eng. Chem. Res.*, 1998, **37**, 2775–2782.
2 J. S. Chung, S. C. Paik, H. S. Kim, D. S. Lee and I. S. Nam, *Catal. Today*, 1997, **35**, 37–43.
3 V. Shinkarev, A. Glushenkov, D. Kuvshinov and G. Kuvshinov, *Carbon*, 2010, **48**, 2004–2012.
4 B. ZareNezhad, *J. Ind. Eng. Chem.*, 2009, **15**, 143–147.
5 X. Zhang, G. Dou, Z. Wang, J. Cheng, H. Wang, C. Ma and Z. Hao, *Catal. Sci. Technol.*, 2013, **3**, 2778–2785.
6 X. Zhang, G. Dou, Z. Wang, L. Li, Y. Wang, H. Wang and Z. Hao, *J. Hazard. Mater.*, 2013, **260**, 104–111.
7 J. S. Eow, *Environ. Prog.*, 2002, **21**, 143–162.
8 P. Van Nisselrooya and J. Lagasb, *Catal. Today*, 1993, **16**, 263–271.
9 X. Wang, T. Sun, J. Yang, L. Zhao and J. Jia, *Chem. Eng. J.*, 2008, **142**, 48–55.
10 E. Alvarez, S. Mendioroz, V. Mun and J. M. Palacios, *Appl. Catal., B*, 1996, **9**, 179–199.
11 A. N. Zagoruiko, V. V. Shinkarev, S. V. Vanag and G. A. Bukhtiyarova, *Catal. Ind.*, 2010, **2**, 343–352.
12 X. Zhang, Z. Wang, N. Qiao, S. Qu and Z. Hao, *ACS Catal.*, 2014, **4**, 1500–1510.
13 X. Zhang, Y. Tang, S. Qu, J. Da and Z. Hao, *ACS Catal.*, 2015, **5**, 1053–1067.
14 X. Zhang, Y. Tang, N. Qiao, Y. Li, S. Qu and Z. Hao, *Appl. Catal., B*, 2015, **176**, 130–138.
15 X. Zhang, Z. Wang, Y. Tang, N. Qiao, Y. Li, S. Qu and Z. Hao, *Catal. Sci. Technol.*, 2015, **5**, 4991–4999.
16 J. Abbasian, A. Rehmat, D. Leppin and D. D. Banerjee, *Fuel Process. Technol.*, 1990, **25**, 1–15.
17 H. Zhang, H. Tong, S. Wang, Y. Zhuo, C. Chen and X. Xu, *Ind. Eng. Chem. Res.*, 2006, **45**, 6099–6103.
18 A. Lancia, D. Musmarra and F. Pepe, *Ind. Eng. Chem. Res.*, 1997, **36**, 197–203.
19 S. J. Lee, S. Y. Jung, S. C. Lee, H. K. Jun, C. K. Ryu and J. C. Kim, *Ind. Eng. Chem. Res.*, 2009, **48**, 2691–2696.
20 Z. Shen, X. Chen, M. Tong, S. Guo, M. Ni and J. Lu, *Fuel*, 2013, **105**, 578–584.
21 Z. Shen, S. Guo, W. Kang, K. Zeng, M. Yin, J. Tian and J. Lu, *Ind. Eng. Chem. Res.*, 2012, **51**, 4192–4198.
22 Y. Jia, Q. Zhong, X. Fan and X. Wang, *Chem. Eng. J.*, 2010, **164**, 132–138.
23 X. Gao, H. Ding, Z. Du, Z. Wu, M. Fang, Z. Luo and K. Cen, *Appl. Energy*, 2010, **87**, 2647–2651.
24 X. Liu, Q. Zhong, J. Wang, X. Ji, Y. Jia, Y. Xu and L. Li, *Energy Sources, Part A*, 2011, **33**, 2027–2035.
25 V. Alopaeus, J. Aittamaa and H. V. Nordén, *Chem. Eng. Sci.*, 1999, **54**, 4267–4271.
26 W. K. Lewis and W. G. Whitman, *Ind. Eng. Chem.*, 1924, **16**, 1215–1220.
27 R. Schneider, E. Kenig and A. Górak, *Chem. Eng. Res. Des.*, 1999, **77**, 633–638.
28 E. Meyer, V. Ermatchkov, Á. P. S. Kamps and G. Maurer, *Fluid Phase Equilib.*, 2006, **244**, 137–152.
29 H. Que and C. C. Chen, *Ind. Eng. Chem. Res.*, 2011, **50**, 11406–11421.
30 Y. Yan and C. Chen, *J. Supercrit. Fluids*, 2010, **55**, 623–634.